Dyes and Pigments 170 (2019) 107608

Contents lists available at ScienceDirect

Dyes and Pigments

journal homepage: www.elsevier.com/locate/dyepig

Simple perylene diimide based polymer acceptor with tuned aggregation for efficient all-polymer solar cells

Zhilin Liu[a,b], Zurong Du[b], Xunchang Wang[b], Dangqiang Zhu[b], Chunming Yang[c,***], Wu Yang[d], Xiaofei Qu[a,**], Xichang Bao[b,*], Renqiang Yang[b]

[a] College of Materials Science and Engineering, Qingdao University of Science and Technology, Qingdao, 266042, China
[b] Qingdao Institute of Bioenergy and Bioprocess Technology, Chinese Academy of Sciences, Qingdao, 266101, China
[c] Shanghai Synchrotron Radiation Facility, Shanghai Advanced Research Institute, Chinese Academy of Sciences, Shanghai, 201204, China
[d] College of Science, Henan University of Technology, Zhengzhou, 450001, China

ARTICLE INFO

Keywords:
Perylenediimide polymer acceptor
All-polymer solar cells
Asymmetric strategy
Fine-tuned aggregation
Power conversion efficiency

ABSTRACT

Polymer acceptors for organic solar cells have got increased attention and becoming a strong candidate to replace small molecular electron acceptors. Here, a polymer acceptor (PBDTβNPDI) was constructed with naphthyl substituted asymmetric benzo [1,2-*b*:4,5-*b*']dithiophene (BDTβN) as donor unit and simple N,N'-Bis(1-propylbutyl)-1,7-dibromoperylene-3,4:9,10-tetracarbox- diimide (PDI) as acceptor unit. The designed polymer has broad absorption spectrum and tuned aggregation with asymmetric donor unit. Then all-polymer solar cells based on PTBTz-2 electron donor and PBDTβNPDI electron acceptor were prepared. The results exhibit that the device has matched energy levels, complementary absorption spectra, and desirable crystallites and nanoscale phase separation, which result in balanced mobility, low weak bimolecular recombination, and thus obtain a remarkable power conversion efficiency of 6.14% with high short circuit current density of 13.89 mA cm^{-2} and decent open circuit voltage of 0.88 V. The results indicate that rational regulation of PDI polymers by asymmetric strategies can obtain ideal polymer accepters, and it has a strong potential to get better results with our in-depth research.

1. Introduction

In recent years, great progresses have been made in the development of polymer solar cells (PSCs). Meanwhile bluk-heterojunction (BHJ) is an optimal structure, because it helps to form nanoscale phase separation photoactive layer, which can result in an ideal device performance due to efficient exciton dissociation and charge transport [1–3]. Now the power conversion efficiencies (PCEs) have been over 10% for fullerene-based solar cells [4,5]. However, the fullerenes and their derivatives (typically $PC_{61}BM$ or $PC_{71}BM$) have distinct drawbacks including poor light absorption in visible and NIR region, difficult energy level regulation, and costly, which absolutely hinder their applications [6]. So, it is a trend to develop high-performance non-fullerene acceptors [7–13]. Among them, polymer acceptors have obvious advantages of easily tunable energy levels and absorption spectra, and also have superior morphological and thermal stability compared to the small molecule counterpart [11–17]. Up to now, the frequently reported polymer acceptors are based on naphthalene and perytene tetracarboxylic diimide (NDI and PDI) [18]. PDI has a large conjugate structure that enables high mobility, suitable energy level, high extinction coefficient, superior thermal and mechanical stability, and process complementary light absorption with most high-performance donor materials at the range of 300–500 nm [15–17,19]. Since 2007, a PDI based polymer acceptor was firstly reported, and the PCE of 1% was obtained in APSCs [20]. After that, lots of polymer acceptors based on PDI were constructed by polymerization with different donor units, such as thiophene, vinylene, fluorene, carbazole, thienylene-vinylene-thienylene, dithiophene, and benzodithiophene [18,21–23]. However, the PCEs of APSCs based on these polymers are only about 5% due to their poor phase separation [24,25]. Even the phase separation of the photoactive layer was further optimized by solvent engineering, the PCEs of the devices are still relatively low [21–25]. Recently, fused perylene diimide (FPDI) with enhanced conjugation structure become a good unit for applications in APSCs. For example, Zhao et al.

* Corresponding author.
** Corresponding author.
*** Corresponding author.
E-mail addresses: yangchunming@zjlab.org.cn (C. Yang), quxiaofei2008@hotmail.com (X. Qu), baoxc@qibebt.ac.cn (X. Bao).

https://doi.org/10.1016/j.dyepig.2019.107608
Received 29 March 2019; Received in revised form 17 May 2019; Accepted 31 May 2019
Available online 07 June 2019

constructed a polymer acceptor NDP-V based on PFDI and vinylene unit, and a high PCE of 8.59% was achieved in APSCs when blended with classical polymer PTB7-th [15]. Zhang et al. obtained a series of FPDI based polymer acceptors through with different donor units, and the PCEs of the related APSCs have reached 6% [26–28]. However, the synthesis of FPDI compounds are much more difficult than that of PDI unit, and the conjugated backbone of PDI can be enough for obtain high mobility polymer acceptor materials. Therefore, it is necessary to deepen understanding the PDI based materials and design more suitable materials to obtain high-performance APSCs.

Here, a novel conjugated polymer acceptor named PBDTβNPDI with naphthyl substituted asymmetric benzo [1,2-b:4,5-b'] dithiophene (BDTβN) as donor unit [29] and simple N,N'-Bis(1-propylbutyl)-1,7-dibromoperylene-3,4:9,10- tetracarboxdiimide as acceptor unit was designed. The obtained polymer has strong absorption in the 300–450 nm wavelength band and tuned aggregation with asymmetric donor unit. Therefore, we successful introduce PTBTz-2 as electron donor in APSCs, which has medium bandgap (~1.72 eV), deep large ionization potential (IP), high extinction coefficient, and planar molecular configuration [30,31]. After synergistic effect of 1, 8-diiodooctane (DIO) and thermal treatment, the APSCs with high PCE of 6.14%, excellent short circuit current density (J_{SC}) of 13.89 mA cm^{-2}, suitable open-circuit voltage (V_{OC}) of 0.87 V, and fill factor (FF) of 50.56% was obtained. The results indicate that the PBDTβNPDI is an ideal acceptor for APSCs, and asymmetric strategy provides a good guideline to design high-performance polymer acceptors.

2. Experimental section

2.1. Materials

Poly (3,4-ethylenedioxythiophene):poly (styrenesulfonate) (PEDOT:PSS 4083) and perylene diimide derivative (PDINO) were obtained from Heraeus (Germany) and Derthon Optoelectronic Materials (Shenzhen, China), and PTBTz-2 and monomer BDTβN were synthesized in our laboratory according to our previous works [29]. The details of synthesis procedure for monomer PDI and polymerization are given in supporting information. Indium tin oxide (ITO) coated glass was bought from Shenzhen display.

2.2. Device fabrication and characterization

ITO-coated glass substrates were cleaned with detergent, deionized water, acetone and isopropyl alcohol in an ultrasonic bath sequentially for 15 min in turn. The cleaned substrates were dried with ultra-pure N_2 flow and treated with O_2 plasma for 6 min. Then, a 30 nm PEDOT: PSS was spin coated on ITO-coated glass at 4000 rpm and baked at 150 °C for 20 min in an oven. After that, the PEDOT:PSS modified ITO-coated glass substrates were transferred into nitrogen-filled glove box. The blend solution of PTBTz-2: PBDTβNPDI was prepared in chrobenzene (CB), and stirring for 5 h. The active layers were spin-coated on the PEDOT:PSS modified ITO-coated glass substrates with different treatment conditions, and PDINO dissolved in methanol (1 mg mL^{-1}, 2300 rpm) was used as buffer layer. Finally, the aluminum layer of about 100 nm as the cathode was thermally evaporated under a vacuum pressure of 4×10^{-4} Pa.

UV–Vis absorption spectra of PBDTβNPDI and PTBTz-2 in thin film were characterized by PerkinElmer Lambda 25 UV/Vis Spectrometer. Cyclic voltammetry (CV) measurements were taken on a CHI660D electrochemical workstation as reported before [30]. The photoluminance spectra were obtained on a Horiba Jobin Yvon FluoroMax-4 Bench-top Spectrofluorometer.

The current density-voltage (*J–V*) characteristics were measured with a Keithley 2420 source measurement unit under simulated 100 mW cm^{-2} (AM 1.5G) irradiation. Light intensity was calibrated with a standard silicon solar cell. External quantum efficiencies (EQEs) were measured using an incident photon-to-charge carrier efficiency (IPCE) setup (7 SC Spec III, Beijing 7-star Optical Instruments Co.) equipped with a standard Si diode. The mobilities were measured using the space-charge-limited current (SCLC) method, and the hole-only device employed a device architecture of ITO/PEDOT:PSS/active layer/Au; electron-only device employed a device architecture of ITO/ZnO/active layer/PDINO/Al. The thicknesses of the active layers were determined by Dektak 150 surface profiler. The morphologies of the films were characterized by a tapping-mode atomic force microscope (AFM, Agilent 5400) and transmission electron microscope (HITACHI H-7650). Grazing incidence wide-angle X-ray scattering (GIWAXS) patterns were acquired by beamline BL16B1 (Shanghai Synchrotron Radiation Facility). The X-ray wavelength was 0.124 nm (E = 10 keV), and the incidence angle was set to 0.2°.

3. Results and discussion

3.1. Synthesis and basic properties

The synthesis route and properties of the polymer PBDTβNPDI is summarized in Scheme S1 and experimental section of supporting information, and the detailrf properties of PTBTz-2 can be find in the previous work [30]. These materials have good solubility in common organic solvents (chloroform, toluene, dichlorobenzene). Furthermore, polymer PBDTβNPD has good thermal stability with the decomposition temperature of 5% weight loss at about 352 °C (Fig. S1), which is enough for practical photovoltaic application. As we know that photovoltaic performance of PSCs not only depends on donor materials but also on acceptor materials [32,33]. Basically, it's a precondition for efficient PSCs which process complementary absorption spectra in the visible and near infrared region (NIR) [34]. Here, Fig. 1a shows the absorption spectra of PBDTβNPDI and PTBTz-2 obtained by UV–Vis method. PTBTz-2 has a broad absorption from 350 to 720 nm, and exhibits strong absorption in the range of 550–680 nm. Furthermore, the PBDTβNPDI presents broad and complementary absorption in the visible range with the optical band gap of 1.63 eV. As a consequence, the blend film covers the range from 350 to 720 nm, which can help the device obtain high J_{SC}.

Easily tunable energy level is another advantageous for non-fullerene acceptors that can obtain matched energy level for realize suitable V_{OC} and offer enough driving force for exciton dissociation. Experimentally, 0.30 eV is an optimal value for the lowest unoccupied molecular orbital (LUMO) offset (ΔLUMO) between donor and acceptor [35–37]. The LUMO and highest occupied molecular orbital (HOMO) energy levels of PTBTz-2 and PBDTβNPDI are given in Fig. 1b and Fig. S2. The LUMO energy level and HOMO energy level of PTBTz-2 and PBDTβNPDI are −3.51 eV, −3.84 eV and −5.40 eV, −5.93 eV, respectively. The ΔLUMO between PTBTz-2 and PBDTβNPDI is 0.33 eV, which supplied sufficient driving force for exciton dissociation. At the same time, the relationship between molecular structure and photovoltaic performance was also investigated by density functional theory method at the B3LYP/6-31G (d,p) level [38,39], as shown in Fig. S3. The dihedral angle of the acceptor is 61.64°, which could limit its self-aggregation tendency to forms a better bicontinuous nanoscale phase separation in photoactive layers.

3.2. Photovoltaic properties

The APSCs were fabricated based on traditional device structure of ITO/PEDOT:PSS/active layer/PDINO/Al (Fig. 1d), and all photovoltaic parameters were recorded under the illumination of AM 1.5G, 100 mW cm^{-2}. The thicknesses of the photoactive layers were controlled in the range of 100–120 nm. The processing conditions were optimized by varying weight ratios, additive concentrations, and thermal treatment conditions. The recorded device parameters of all solar cells are listed in Fig. 2, Figs. S4,5,7, Table 1, and Tables S1–S4. In

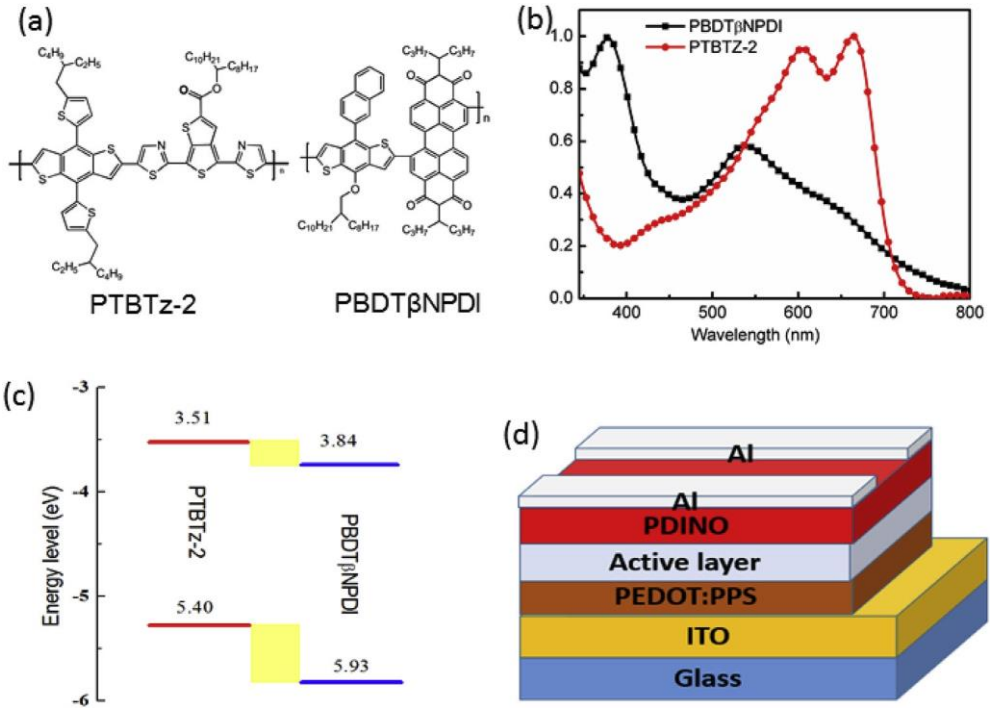

Fig. 1. The molecular structure of PTBTz-2 and PBDTβNPDI (a), UV–Vis absorption spectra of the PTBTz-2 and PBDTβNPDI film (b), energy levels of PTBTz-2 and PBDTβNPDI (c), and device structure (d).

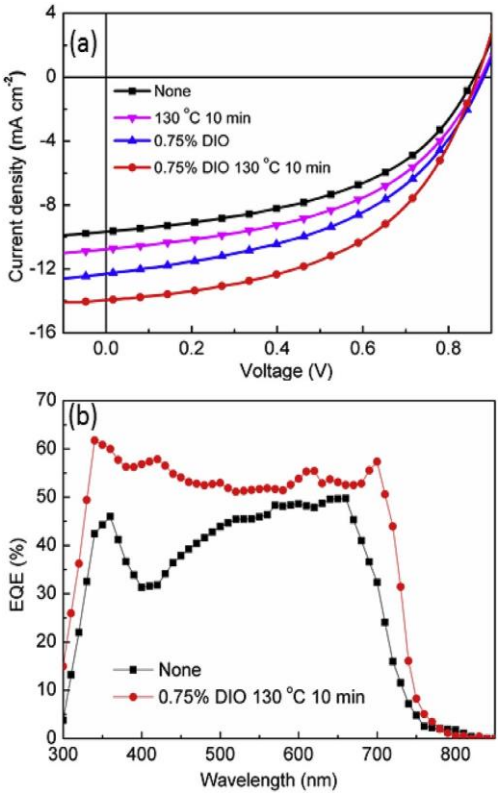

Fig. 2. *J-V* curves of the photovoltaic devices under different conditions (a), and EQE curves without treatment and under optimal condition (b).

most cases, the commonly used D/A weight ratio for non-fullerene solar cells is 1:1. Firstly, the APSCs based on the fixed weight ratio of D/A at 1:1 without any treatment were fabricated and the device exhibits the PCE of 3.93% with J_{SC} of 9.59 mA cm^{-2}, V_{OC} of 0.86 V, and FF of 47.26%. Commonly, introducing additive is a useful method to improve PCE, because it can change the phase separation of the photoactive layers and thus balance and/or enhance carrier mobility. However, it has a negative influence on device performance when chloronaphthalene (CN) was introduced (Table S1). But thermal treatment has positive effect on the devices under same amount of CN additive, and further confirms without additives (Fig. S4 and Table S2). The PCE of the device is increased to 4.52% with J_{SC} of 10.74 mA cm^{-2}, V_{OC} of 0.87 V, and FF of 48.15% only under 130 °C for 10 min. On contrast, it clearly to find that DIO additive has positive influence on photovoltaic performance (Fig. S5 and Table S3). When 0.75% DIO was added, the PCE of the APSCs is increased to 5.07% with V_{OC} of 0.88 V, J_{SC} of 12.27 mA cm^{-2} and FF of 46.92%. However, the PCE of the device suffers a remarkable decrease when added 1.0% DIO due to poor phase separation that may be result in decreased charge transport (Fig. S6). After that, we further optimized the process by synergistic use of 0.75% DIO and thermal treatment at 130 °C for 10 min. It is amazing to find that the PCE reaches 6.14% with J_{SC} of 13.89 mA cm^{-2}, V_{OC} of 0.87 V, and FF of 50.56%. In addition, the devices under different weight ratios based on the optimal process condition were also investigated (Fig. S7 and Table S4). The results show that the photoactive layer based on optimal weight ratio of 1:1 forms an ideal charge-transporting network.

The device performance processed under optimal condition get an impressive improvement mainly ascribed to high J_{SC}, and the results were further confirmed by the external quantum efficiency (EQE) curves (Fig. 2b). The devices show a broad photoresponse in the range from 350 to 750 nm whether process under optimal condition or not, which agrees with the absorption spectrum of photoactive layer as discussed above. The device without treatment suffers relative poor photoresponse in short wavelength region (~300–550 nm). But the optimal device exhibits good photoresponse, especially in the short wave region, and the best EQE value of the optimal device is higher than 60%. This broad and good photoresponse is responsible for the improved J_{SC}.

Table 1
The device parameters under different treatment conditions.

Conditions	V_{OC} (V)	J_{SC} (mA cm^{-2})	FF (%)	PCE_{max}/PCE_{ave} (%)[a]	μ_h ($cm^2 V^{-1} S^{-1}$)	μ_e ($cm^2 V^{-1} S^{-1}$)	μ_h/μ_e	R_S (Ω)[b]	R_{sh} (Ω)[b]
None	0.86 (0.86 ± 0.01)	9.59 (9.47 ± 0.15)	47.26 (45.02 ± 2.85)	3.93 (3.67 ± 0.27)	9.88×10^{-5}	6.17×10^{-5}	1.60	21.1	407.1
130 °C	0.87 (0.87 ± 0.01)	10.74 (10.55 ± 0.19)	48.15 (47.30 ± 0.85)	4.52 (4.41 ± 0.11)	1.49×10^{-5}	9.68×10^{-5}	1.54	19.1	385.4
0.75% DIO	0.88 (0.87 ± 0.01)	12.27 (11.38 ± 0.89)	46.92 (44.36 ± 2.56)	5.07 (4.69 ± 0.38)	1.28×10^{-5}	8.32×10^{-5}	1.54	17.3	304.2
0.75% DIO 130 °C	0.87 (0.87 ± 0.01)	13.89 (13.78 ± 0.12)	50.56 (49.78 ± 0.78)	6.14 (6.02 ± 0.12)	1.61×10^{-4}	1.22×10^{-4}	1.31	13.6	421.4

[a] The average values are obtained from 10 separate devices.
[b] The values are obtained from J-V curves of the device under illumination.

3.3. Space charge-limited current

To deepen understand the influence of process conditions on J_{SC}, the space charge limited current (SCLC) methods were used to investigate the mobilities (hole mobility μ_h and electron mobility μ_e) of the blend films. The $J-V$ curves under dark condition are shown in Figs. S8 and S9, and the calculated hole and electron mobilities are given in Table 1. The μ_h and μ_e of the blend film without any treatment are 9.88×10^{-5} $cm^2V^{-1}s^{-1}$ and 6.17×10^{-5} $cm^2V^{-1}s^{-1}$, respectively, and the ratio value of μ_h/μ_e is 1.60. As expected, the values of μ_h and μ_e have slight increase after the addition of 0.75% DIO or thermal treatment at 130 °C for 10 min. And the ratio value of μ_h/μ_e decrease to same value of 1.54, much balanced charge transport will help to reduce charge accumulation as well as recombination. After combination treatment with the addition of 0.75% DIO and thermal treatment at 130 °C for 10 min, the μ_h and μ_e are increased to 1.61×10^{-4} $cm^2V^{-1}s^{-1}$ and 1.27×10^{-4} $cm^2V^{-1}s^{-1}$, respectively, and the μ_h/μ_e value is 1.31. The results reveal that the synergistic effect of DIO additive and thermal treatment can further balance the mobilities between electrons and holes, which is essential for high-performance organic solar cells [30,40,41]. However, the relative poor FF for all devices may be ascribed to large interface series resistance (R_s) and small shunt resistance (R_{sh}) (Table 1) [42,43].

3.4. Charge recombination

Photocurrent density (J_{ph}) and corresponding effective voltage (V_{eff}) curves of the APSCs were also investigated, as shown in Fig. 3a. Obviously, J_{ph} presents a linear function at the low value of V_{eff}, and become saturate when the value of V_{eff} is high enough. Historically, saturated photocurrent density (J_{sat}) defined as $J_{sat} = qG_{max}L$, (G_{max} defined as the maximum exciton generation rate), thus the G_{max} of the APSCs without treatment and under optimal condition are $4.6 \times 10^{-29} m^{-3}s^{-1}$, and $5.3 \times 10^{-29} m^{-3}s^{-1}$, respectively. The results show that exciton generation of the APSCs has greatly increased under the synergistic effect of DIO and thermal treatment. What's more, J_{ph} for APSCs can also been defined by equation of $J_{ph} = qG_{max}P(E, T)L$, and P (E,T) defined as exciton dissociation probabilities. As shown in Fig. 3b, the P (E,T) is increased from 71% to 83%, when introduce 0.75% DIO additive and thermal treatment at 130 °C for 10 min, suggesting that it is an effective method to improve the probability of exciton generation and dissociation.

The charge recombination mechanism of the APSCs was also studied by using J_{SC} and V_{OC} values of the APSCs under different illumination light intensities (P) (Fig. S10). Usually, the value of J_{SC} and P follows a power-law relationship of $J_{SC} \propto P^S$,. The closer the S value is to 1, there have weak bimolecular recombination in photoactive layer. From Fig. 4c, the fitted slope value of the device without treatment and under optimal condition is 0.978 and 0.984, which shows that the recombination can be suppressed after post treatment. Furthermore, the relationship between V_{OC} value and P is following the formula: $V_{OC} \propto \frac{nkT}{q}\ln(P)$ [44,45], where n is an indicator of recombination mechanism, k is Boltzmann constant, T is Kelvin temperature. When n is 1, it would be free of bimolecular recombination, when n = 2, there should exist strong trap-assisted recombination. As can be seen from Fig. 3d, the APSCs without treatment exhibits the slope of 1.246kT/q, and the slope of the optimal device is only 1.061kT/q. This finding also shows that addition of DIO into solution and thermal treatment can further tune the photoactive layers and reduce bimolecular recombination, which help to obtain high-performance devices.

3.5. Morphological and assemble properties

To explore the relationship between blend morphology and their photovoltaic performance, a series of tests were conducted. Firstly, atom force microscopy (AFM) was employed to study surface

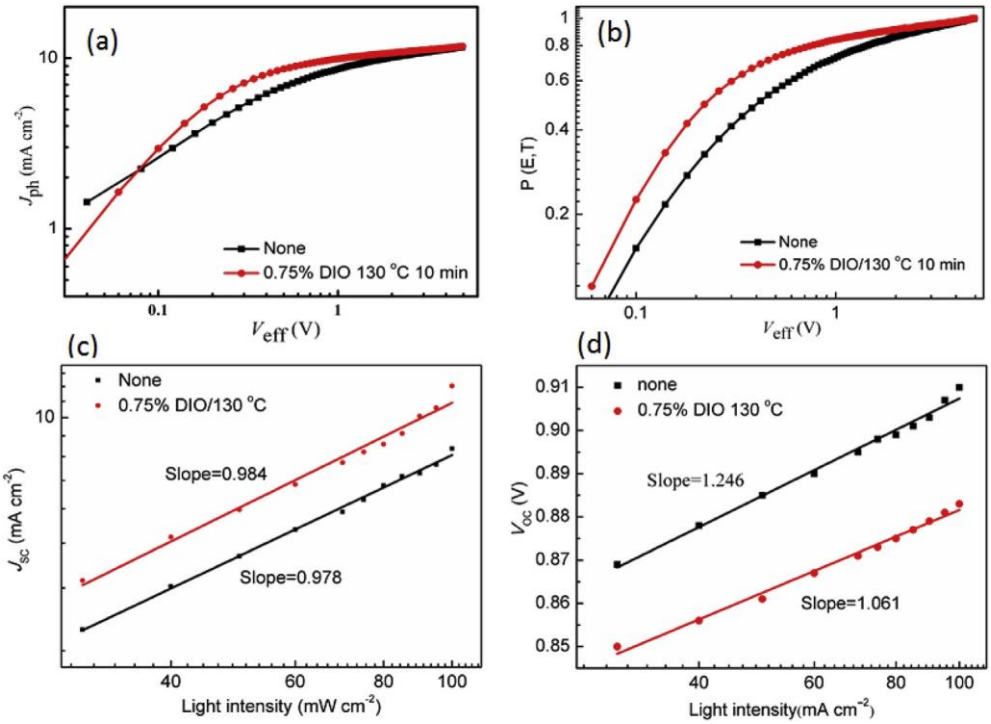

Fig. 3. Photocurrent density of the APSCs and their P (E, T) curves (a, b); and J_{SC} and V_{OC} versus light intensity curves.

information of the photoactive layers. As shown in Fig. 4, the blend film without treatment owns a smooth surface with a root-mean-square (RMS) value of 0.75 nm. It means that the blend film manifests a week aggregation. As expected, the RMS value is gradually increased to 1.08 nm when the blend film treated with thermal treatment and added 0.75% DIO, suggesting that the aggregation is enhanced. The enhanced aggregation of the polymer can increase the charge transport and thus improve device performance. As we know that AFM can only offer surface information, and then transmission electron microscopy (TEM) was applied to investigate in-depth morphology of the photoactive layers. The blend film without treatment exhibits few amount of interconnect polymer nanofibers (Fig. 4e). However, the films treated with 0.75% DIO or thermal treatment exhibit increased fibril-like aggregation (Fig. 4f and g). Interestingly, the blend film treated with the synergistic effect of DIO and thermal treatment, a better phase separated as well as more apparent network was observed, which benefit to

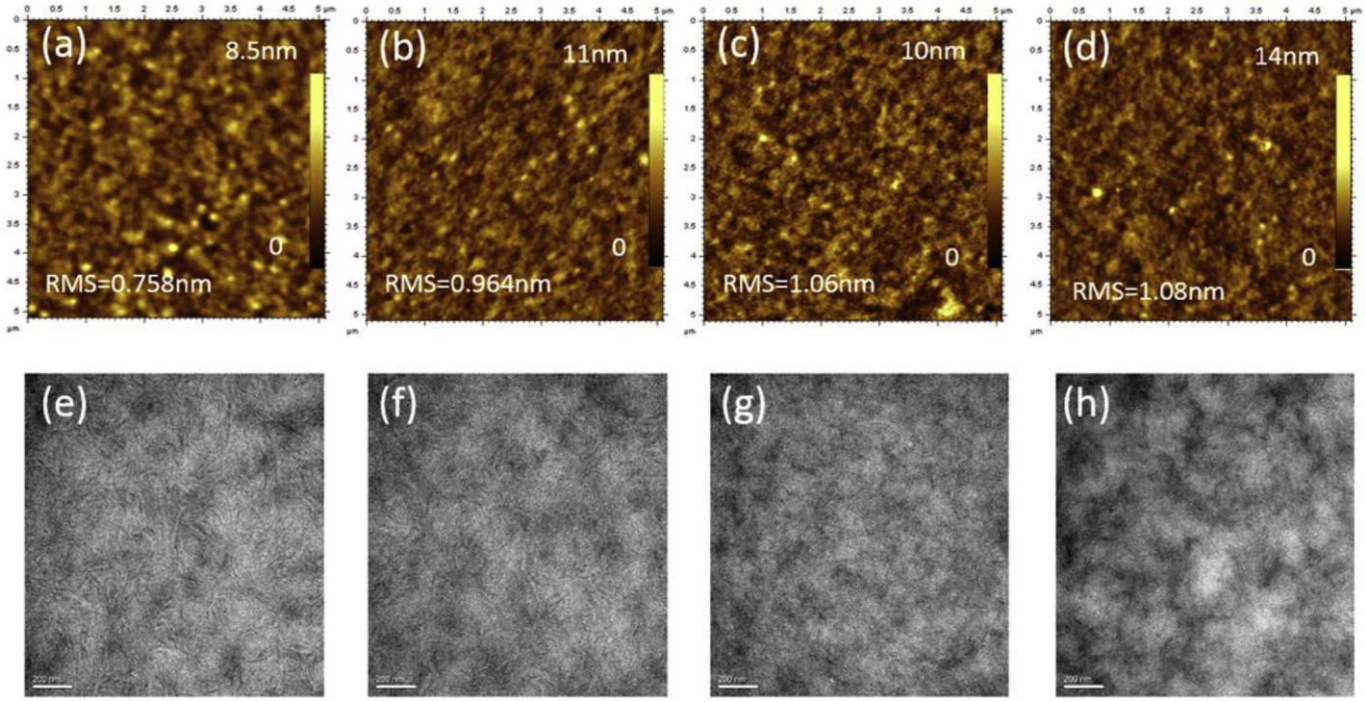

Fig. 4. AFM (a–d) and TEM (e–h) images (e–f) of the blend films. (a) and (e) none, (b) and (f) with 0.75% DIO, (c) and (g) thermal treatment at 130 °C for 10min, (d) and (h) with 0.75% DIO and thermal treatment at 130 °C for 10 min.

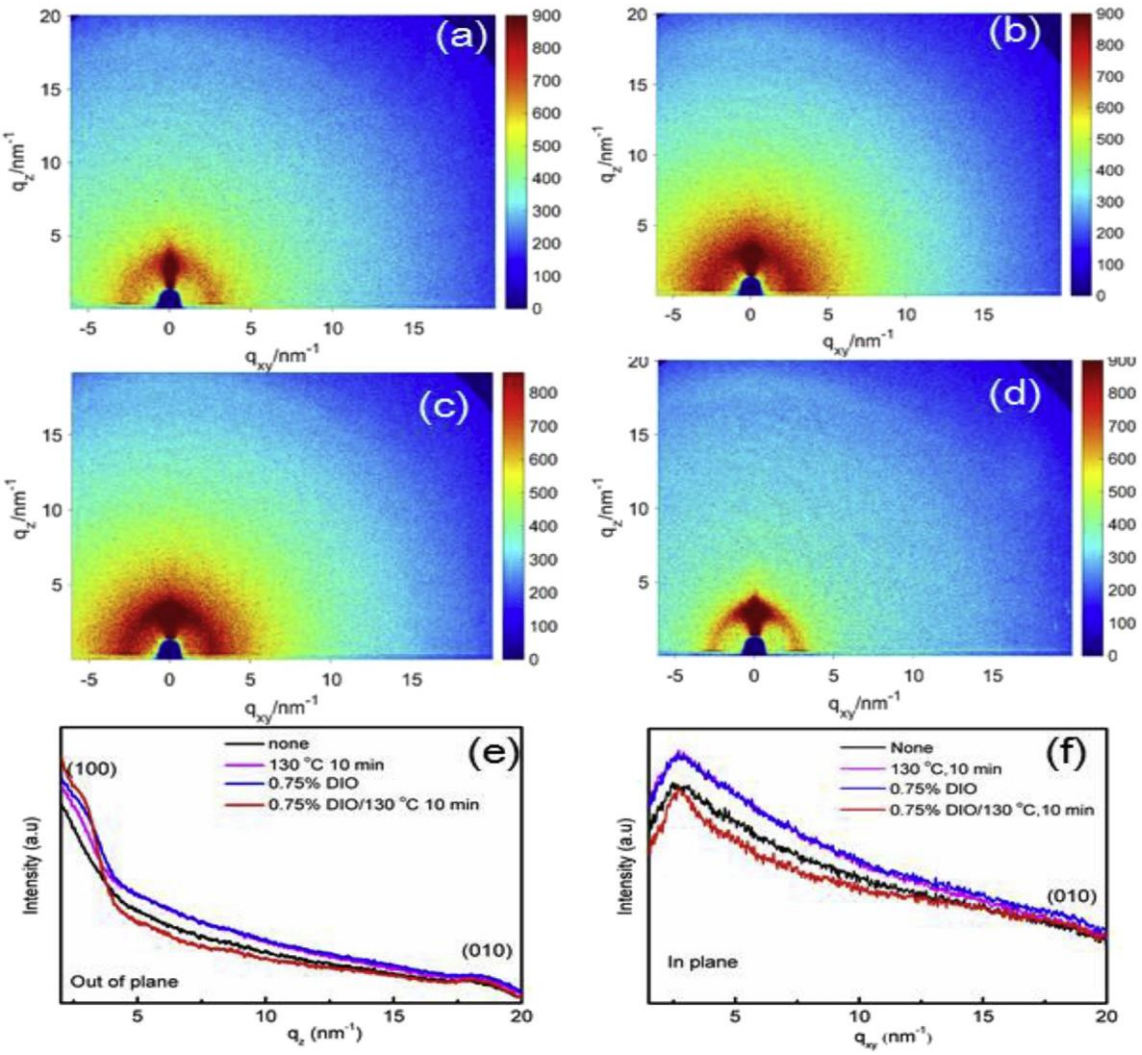

Fig. 5. (a) 2D-GIWAXS images of the blend films treated with different conditions, (a) none, (b) 130 °C, 10 min, (c) 0.75% DIO, (d) 0.75% DIO/130 °C, 10 min, and 1D profiles integrated from 2D patterns on out-of-plane (e) and in-plane (f) directions.

exciton dissociation and charge transport. This is the main reason to the remarkable increased J_{SC} and PCE.

In order to confirm the above results, grazing incidence wide-angle X-ray diffraction (GIWAXS) method was used to study molecular packing information. Two-dimensional (2D) GIWAXS patterns (a-d) of the blend films under different conditions and their one-dimensional GIWAXS profiles (e, f) integrated from 2D patterns on the out-of-plane and in-plane directions are given in Fig. 5 and Fig. S11. It can be seen that there have lamellar stacking peaks and π-π stacking peaks in all blend films under different treatment conditions, which mainly ascribed to PTBTz-2. In details from Fig. 5 (e, f), the blend films exhibit (100) diffractions in both q_z and q_{xy} direction at 2.54 nm^{-1} and the intense (010) diffraction at $q_z = 18$ nm^{-1}, which calculated $d_{100} = 2.47$ nm and $d_{010} = 0.34$ nm respectively. Furthermore, the blend film without treatment exhibits a week (100) reflection peak in the out-of-direction, and this peak has a slightly enhanced after treatment at 130 °C for 10 min or add 0.75% DIO. Moreover, the blend film with the addition of 0.75% DIO and thermal treatment at 130 °C for 10 min shows stronger (100) peaks in q_z direction, and the peak (010) in plane direction is also enhanced under optimal condition, indicates a desirable crystalline behavior, an essential factor to enhance exciton dissociation and charge transport, and thus improve device performance.

4. Conclusion

A novel polymer acceptor PBDTβNPDI was designed and synthesized with broad absorption spectrum and tuned aggregation, and then we fabricate APSCs by introduce PTBTz-2 as electron donor. The PTBTz-2 and PBDTβNPDI reveal a complementary absorption. Meanwhile, the blend film has matched energy level and suitable LUMO offset of 0.33 eV for exciton separation. Moreover, the crystallites and phase separation of the polymer donor and acceptor can be fine-tuned by the synergistic effect of DIO additive and thermal treatment. All these effects make the device has balanced mobility, low weak bimolecular recombination. Consequently, high-performance APSC with the PCE of 6.14%, excellent J_{SC} of 13.89 mA cm^{-2} and large V_{OC} of 0.88 V was obtained. The findings show that PBDTβNPDI is an ideal acceptor for APSCs, and asymmetric strategy provides a good guideline to design high-performance polymer acceptors.

Acknowledgements

This work was supported by the National Natural Science Foundation of China (61504073, 51573205), the National Key R&D Program of China (2017YFA0403000), Science and Technology Commission of Shanghai Municipality (17JC1400802), and the Natural Science Foundation of Henan Province (182300410195). X. Bao thanks

the Youth Innovation Promotion Association CAS (2016194) for financial support. The authors thank beamline BL16B1 (Shanghai Synchrotron Radiation Facility) for providing beam time.

Appendix A. Supplementary data

Supplementary data to this article can be found online at https://doi.org/10.1016/j.dyepig.2019.107608.

Rerferences

[1] Hu H, Li Y, Zhang J, Peng Z, Ma L, Xin J, et al. Effect of ring-fusion on miscibility and domain purity: Key factors determining the performance of PDI-based non-fullerene organic solar cells. Adv Energy Mater 2018;8:1800234.
[2] Liu T, Huo L, Chandrabose S, Chen K, Han G, Qi F, et al. Optimized fibril network morphology by precise side-chain engineering to achieve high-performance bulk-heterojunction organic solar cells. Adv Mater 2018;30:1707353.
[3] Li J, Wang Y, Liang Y, Wang N, Tong J, Yang C, et al. Enhanced organic photovoltaic performance through modulating vertical composition distribution and promoting crystallinity of the photoactive layer by diphenyl sulfide additives. ACS Appl Mater Interfaces 2019;11:7022–9.
[4] He Z, Xiao B, Liu F, Wu H, Yang Y, Xiao S, et al. Single-junction polymer solar cells with high efficiency and photovoltage. Nat Photon 2015;9:174–9.
[5] Chen J, Cui C, Li Y, Zhou L, Ou Q, Li C, et al. Single-Junction polymer solar cells exceeding 10% power conversion efficiency. Adv Mater 2015;27:1035–41.
[6] Cheng P, Li G, Zhan X, Yang Y. Next-generation organic photovoltaics based on non-fullerene acceptors. Nat Photon 2018;12:131–42.
[7] Lin Y, Wang J, Zhang ZG, Bai H, Li Y, Zhu D, et al. An electron acceptor challenging fullerenes for efficient polymer solar cells. Adv Mater 2015;27:1170–4.
[8] Yan C, Barlow S, Wang Z, Yan H, Jen A, Marder S, et al. Non- fullerene acceptors for organic solar cells. Nat Rev Mater 2018;3:18003.
[9] Liu Z, Wu Y, Zhang Q, Guo X. Non-fullerene small molecule acceptors based on perylene diimides. J Mater Chem 2016;4:17604–22.
[10] Zhou N, Dudnik A, Li T, Manley E, Aldrich T, Guo P, et al. All-polymer solar cell performance optimized via systematic molecular weight tuning of both donor and acceptor polymers. J Am Chem Soc 2016;138:1240–51.
[11] Yang J, Xiao B, Tajima K, Nakano M, Takimiya K, Tang A, et al. Comparison among perylene diimide (PDI), naphthalene diimide (NDI), and naphthodithiophene diimide (NDTI) based n-type polymers for all-polymer solar cells application. Macromolecules 2017;50:3179–85.
[12] Gao L, Zhang Z, Xue L, Min J, Zhang J, Wei W, et al. All-polymer solar cells based on absorption-complementary polymer donor and acceptor with high power conversion efficiency of 8.27%. Adv Mater 2016;28:1884–90.
[13] Liu X, Zhang C, Duan C, Li M, Hu Z, Wang J, et al. Morphology optimization via side chain engineering enables all polymer solar cells with excellent fill factor and stability. J Am Chem Soc 2018;14:8934–43.
[14] Liu X, Zou Y, Wang H, Wang L, Fang J, Yang C. High-performance all-polymer solar cells with a high fill factor and a broad tolerance to the donor/acceptor ratio. ACS Appl Mater Interfaces 2018;10:38302–9.
[15] Guo Y, Li Y, Awartani O, Han H, Zhao J, Ade H, et al. Improved performance of all-polymer solar cells enabled by naphthodipery- lenetetraimide-based polymer acceptor. Adv Mater 2017;29:1700309.
[16] Guo Y, Li Y, Awartani O, Zhao J, Han H, Ade H, et al. A vinylene-bridged perylenediimide-based polymeric acceptor enabling efficient all-polymer solar cells processed under ambient conditions. Adv Mater 2016;28:8483–9.
[17] Cheng P, Ye L, Zhao X, Hou J, Li Y, Zhan X. Binary additives synergistically boost the efficiency of all-polymer solar cells up to 3.45%. Energy Environ Sci 2014;7:1351–6.
[18] Yang J, Xiao B, Tang A, Li J, Wang X, Zhou E. Aromatic-diimide-based n-type conjugated polymers for all-polymer solar cell applications. Adv Mater 2018;30:1804699.
[19] Zhan X, Facchetti A, Barlow S, Marks TJ, J.T, Ratner MA, et al. Adv Mater 2011;23:268–84.
[20] Zhan X, Tan Z, Domercq B, An Z, Zhang X, Barlow S, et al. A high-mobility electron-transport polymer with broad absorption and its use in field-effect transistors and all-polymer solar cells. J Am Chem Soc 2007;129:7246–7.
[21] Chang H, Chen Z, Yang X, Yin Q, Zhang J, Ying L, et al. Novel perylene diimide based polymeric electron-acceptors containing ethynyl as the p-bridge for all-polymer solar cells. Org Electron 2017;45:227–33.
[22] Zhang Y, Guo X, Su W, Guo B, Xu Z, Zhang M, et al. Perylene diimide-benzodithiophene D-A copolymers as acceptor in all-polymer solar cells. Org Electron 2017;41:49–55.
[23] Deng P, Wu B, Lei Y, Zhou D, Ho CHY, Zhu F, et al. A readily- accessible, random perylene diimide copolymer acceptor for all-polymer solar cells. Dyes Pigments 2017;146:20–6.
[24] Liao X, Zhao X, Zhang Z, Wnag H, Zhan X, Li Y, et al. All-polymer solar cells based on side-chain-isolated polythiophenes and poly(perylene diimide-alt-dithienothiophene). Sol Energy Mater Sol Cell 2013;117:336–42.
[25] Yuan J, Xu Y, Shi G, Ling X, Ying L, Huang F, et al. Engineering the morphology via processing additives in multiple all-polymer solar cells for improved performance. J Mater Chem A 2018;6:10421–32.
[26] Yin Y, Yang J, Guo F, Zhou E, Zhao L, Zhang Y. High-performance all-polymer solar cells achieved by fused perylenediimide-based conjugated polymer acceptors. ACS Appl Mater Interfaces 2018;10:15962–70.
[27] Liu M, Yang J, Yin Y, Zhang Y, Zhou E, Guo F, et al. Novel perylenediimide-based polymers with electron-deficient segment as the comonomer for efficient all-polymer solar cells. J Mater Chem 2018;6:414–22.
[28] Liu M, Yang J, Lang C, Zhang Y, Zhou E, Liu Z, et al. Fused perylenediimide-based polymeric acceptors for efficient all-polymer solar cells. Macromolecules 2017;50:7559–66.
[29] Liu D, Gu C, Wang J J, Zhu D, Li Y, Bao X, et al. Naphthalene substituents bonded via the bposition: an extended conjugated moiety can achieve a decent trade-off between optical band gap and open circuit voltage in symmetry-breaking benzodithiophene-based polymer solar cells. J Mater Chem 2017;5:9141–7.
[30] Zhu D, Bao X, Zhu Q, Gu C, Qiu M, Wen S, et al. Thienothiophene-based copolymers for high-performance solar cells, employing different orientations of the thiazole group as a pi bridge. Energy Environ Sci 2017;10:614–20.
[31] Bao X, Zhang Y, Wang J, Zhu D, Yang C, Li Y, et al. High extinction coefficient thieno 3,4-b thiophene-based copolymer for efficient fullerene-free solar cells with large current density. Chem Mater 2017;29:6766–71.
[32] Lian X, Zhang L, Hu Y, Zhang Y, Yuan Z, Zhou W, et al. Effect of substituents of twisted benzodiperylenediimides on non-fullerene solar cells. Org Electron 2017;47:72–8.
[33] Dou K, Wang X, Du Z, Jiang H, Li F, Sun M, et al. Synergistic effect of side-chain and backbone engineering in thieno 2,3-f benzofuran-based conjugated polymers for high performance non-fullerene organic solar cells. J Mater Chem A 2019;7:958–64.
[34] Li J, Liang Z, Wang Y, Li H, Tong J, Bao X, et al. Enhanced efficiency of polymer solar cells through synergistic optimization of mobility and tuning donor alloys by adding high-mobility conjugated polymers. J Mater Chem C2018;6:11015–22.
[35] Bredas J, Beljonne D, Coropceanu V, Cornil J. Charge-transfer and energy-transfer processes in pi-conjugated oligomers and polymers: a molecular picture. Chem Rev 2004;104:4971–5003.
[36] Scharber M, Wuhlbacher D, Koppe M, Denk P, Waldauf C, Heeger A, et al. Design rules for donors in bulk-heterojunction solar cells - towards 10 % energy-conversion efficiency. Adv Mater 2006;18:789–94.
[37] Gong X, Tong M, Brunetti F, Seo J, Sun Y, Moses D, et al. Heeger bulk heterojunction solar cells with large open-circuit voltage: electron transfer with small donor-acceptor energy offset. Adv Mater 2011;23:2272–7.
[38] Lee C, Yang W, Parr R. Develoopment of the colle-savetti correlation- energy formula into a functional of the electron density. Phys Rev B 1988;37:785–9.
[39] Becke A. Density-functional exchange-energy approximation with correct asymptotic behevior. Phys Rev 1988;38:3098–100.
[40] Zhang L, Xu X, Lin B, Zhao H, Li T, Xin J, et al. Achieving balanced crystallinity of donor and acceptor by combining blade-coating and ternary strategies in organic solar cells. Adv Mater 2018;30:1805041.
[41] Wen S, Li Y, Rath T, Li Y, Wu Y, Bao X, et al. A benzobis(thiazole)-based copolymer for highly efficient NonFullerene polymer solar cells. Chem Mater 2019;31:919–26.
[42] Servaites J, Yeganeh S, Marks T, Ratner M. Efficiency enhancement in organic photovoltaic cells: consequences of optimizing series resistance. Adv Funct Mater 2010;20:97–104.
[43] Street R, Song K, Cowan S. Influence of series resistance on the photocurrent analysis of organic solar cells. Org Electron 2011;12:244–8.
[44] Schilinsky P, Waldauf C, Brabec C. Recombination and loss analysis in polythiophene based bulk heterojunction photodetectors. Appl Phys Lett 2002;81:3885–7.
[45] Mihailetchi V, Xie H, Boer B, Koster L, Blom P. Charge transport and photocurrent generation in poly (3-hexylthiophene): methanofullerene bulk-heterojunction solar cells. Adv Funct Mater 2006;16:699–708.